Analytical methods for the mechanics of graphene bubbles

Kaimin Yue, Wei Gao, Rui Huang, and Kenneth M. Liechti

Related Articles

Internal friction and dynamic modulus in Ru-50Nb ultra-high temperature shape memory alloys
Appl. Phys. Lett. 101, 161909 (2012)

A continuum glassy polymer model applicable to dynamic loading
J. Appl. Phys. 112, 083511 (2012)

Effects of mechanical contact stress on magnetic properties of ferromagnetic film
J. Appl. Phys. 112, 084901 (2012)

Pyramidal dislocation induced strain relaxation in hexagonal structured InGaN/AlGaN/GaN multilayer
J. Appl. Phys. 112, 083502 (2012)

Resonant frequency analysis of Timoshenko nanowires with surface stress for different boundary conditions
J. Appl. Phys. 112, 074322 (2012)

Additional information on J. Appl. Phys.

Journal Homepage: http://jap.aip.org/

Journal Information: http://jap.aip.org/about/about_the_journal

Top downloads: http://jap.aip.org/features/most_downloaded

Information for Authors: http://jap.aip.org/authors

Analytical methods for the mechanics of graphene bubbles

Kaimin Yue, Wei Gao, Rui Huang,[a] and Kenneth M. Liechti
Research Center for the Mechanics of Solids, Structures and Materials, Department of Aerospace Engineering and Engineering Mechanics, University of Texas, Austin, Texas 78712, USA

When placing a graphene membrane on a substrate, gas molecules may be trapped underneath to form bubbles. The size of a graphene bubble (e.g., diameter and height) depends on the number of gas molecules that are trapped, the elastic properties of graphene, and the interfacial adhesion between graphene and the substrate. A mechanics analysis of such graphene bubbles is conducted via membrane and nonlinear plate theories, so that the interfacial adhesion can be determined directly from measurements of the bubble size. A comparison of the results from these two models establishes that the membrane analysis is sufficient for relatively large bubbles. The adhesion energy of mechanically exfoliated graphene on silicon oxide is extracted from two reported data sets using the simple membrane theory, and the values range from 0.097 to 0.43 J/m^2. Moreover, the strain distribution of the graphene bubbles and transport of gas molecules among the bubbles are discussed. © *2012 American Institute of Physics*. [http://dx.doi.org/10.1063/1.4759146]

I. INTRODUCTION

Graphene bubbles have been observed in experiments. Stolyarova *et al.*[1] observed nanoscale bubbles when mechanically exfoliated graphene flakes were placed on top of a silicon substrate covered with a thermally grown silicon oxide layer and exposed to proton irradiation. Much larger graphene bubbles were observed when the graphene flakes were exposed to vapors of hydrofluoric acid (HF) and water. In both cases, gas was released from the silicon oxide and trapped underneath the impermeable graphene, resulting in formation of the bubbles. More recently, Georgiou *et al.*[2] reported that bubbles are regularly found at the silicon oxide/graphene interface in large flakes obtained by mechanical cleavage. They observed graphene bubbles with diameters ranging from tens of nanometers to tens of microns and a variety of shapes (circular, triangular, and diamond). Bubbles have also been observed in graphene grown on a Pt (111) substrate.[3] While the origin of graphene bubbles has not been fully understood and may vary with the material systems and experimental conditions, several potential applications of the graphene bubbles have emerged. Using highly strained graphene nanobubbles, Levy *et al.*[3] demonstrated enormous pseudo-magnetic fields and suggested strain engineering as a viable means of mechanical control over electronic structure of graphene. Georgiou *et al.*[2] demonstrated controllable curvature of graphene bubbles by applying an external electric field, which may be used as optical lenses with variable focal length. Zabel *et al.*[4] used graphene bubbles to study the Raman spectrum of graphene under biaxial strain. A well-controlled pressurization method was developed by Bunch *et al.*[5] to form graphene bubbles (or balloons) on patterned substrates, which was used to demonstrate the impermeability of graphene to gas molecules and to measure elastic properties of graphene. Following a similar approach, Koenig *et al.*[6] measured the adhesion energy between graphene and silicon oxide. On the other hand, Zong *et al.*[7] used intercalation of nanoparticles to generate graphene blisters on silicon surfaces and thereby provided a measurement of the graphene adhesion.

The present study focuses on the mechanics of graphene bubbles in order to establish a theoretical relationship between the morphology of graphene bubbles and the mechanical as well as interfacial properties of graphene. We show that, with known elastic properties of graphene, the adhesion energy between graphene and its substrate can be determined from the measurable dimensions of a graphene bubble (e.g., diameter and height). The number of gas molecules inside the bubble and the pressure can be determined simultaneously. Moreover, we confirm that the strain of graphene is nonuniform, varying from an equibiaxial strain at the center of the bubble to a uniaxial strain at the edge. The magnitude of the strain depends on the adhesion energy, but is independent of the bubble size. The mechanics of graphene bubbles is then extended to discuss transport of gas molecules among graphene bubbles of different sizes and the coalescence of graphene bubbles from a thermodynamics perspective.

The remainder of this paper is organized as follows. Section II presents an analysis of graphene bubbles based on a membrane theory that neglects the bending stiffness of graphene. In Sec. III, we take into account the bending stiffness of graphene by conducting an analysis based on the nonlinear plate theory. The results are compared with reported experimental data in Sec. IV, along with discussions on applications for measurements of adhesion energy, strain, and transport of gas molecules. The effect of van der Waals interaction is briefly discussed, with comments on the difference between microbubbles and nanobubbles. The conclusions are drawn in Sec. V.

II. A MEMBRANE ANALYSIS

Similar to the pressurized thin film blisters,[8] the mechanics of graphene bubbles can be analyzed by using either membrane or nonlinear plate theories. The former ignores the

---

[a]Author to whom correspondence should be addressed. Electronic mail: ruihuang@mail.utexas.edu.
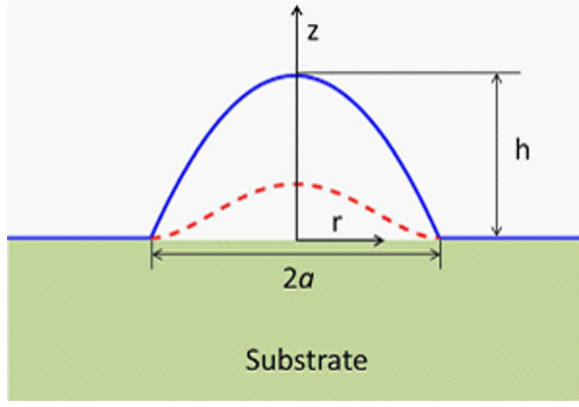
FIG. 1. Schematic illustration for the shapes of large and small graphene bubbles as, respectively, analyzed by membrane (blue, solid line) and plate theories (red, dashed line).

bending stiffness of the film, giving rise to relatively simple solutions. In the present study, we compare the two types of theoretical analyses and establish the conditions for the sufficiency of the membrane analysis.

Figure 1 illustrates two shapes of graphene bubbles. In the elastic plate theory, the edge of the bubble is clamped with zero slope due to a finite bending stiffness. In the membrane analysis, the boundary condition at the edge is relaxed, resulting in a kink (infinite curvature) at the edge. Typically, it is expected that the plate theory (with nonlinear effects) is more accurate but also more tedious for numerical analysis. When the bubble size is large, the membrane theory is expected to provide a good approximation with relatively simple analysis. For an elastic thin film to be treated as a membrane, the central deflection should be at least several times of the film thickness.[8] For a monolayer graphene, however, its thickness is not well defined[9] and the critical dimension for the membrane analysis has to be established by comparing to the nonlinear plate theory.

Consider an axisymmetric bubble with radius a and central deflection h (Fig. 1). In the membrane analysis, the deflection profile is assumed to be

$$z(r) = h \left(1 - \frac{r^2}{a^2} \right),\tag{1}$$

which is approximately a spherical cap for relatively small h compared to a. In addition, for the deformation to be kinematically admissible, a radial displacement is assumed

$$u(r) = u_0 \frac{r}{a} \left(1 - \frac{r}{a} \right),\tag{2}$$

where u_0 is a parameter to be determined. Note that the assumed deformation in Eqs. (1) and (2) is generally considered as a reasonable approximation for moderately large bubbles.

With the deformation of graphene described by Eqs. (1) and (2), the radial and circumferential strain components are obtained as

$$\varepsilon_r(r) = \frac{u_0}{a} \left(1 - \frac{2r}{a} \right) + \frac{2h^2 r^2}{a^4},\tag{3}$$

$$\varepsilon_\theta(r) = \frac{u_0}{a} \left(1 - \frac{r}{a} \right).\tag{4}$$

Note that the circumferential strain is necessarily zero at the edge ($r = a$) under the condition that the graphene membrane outside the bubble ($r > a$) is attached to the substrate with no deformation or sliding.

The elastic strain energy per unit area of the membrane is

$$U(r) = \frac{E_{2D}}{2(1 - v^2)} (\varepsilon_r^2 + 2v\varepsilon_r\varepsilon_\theta + \varepsilon_\theta^2),\tag{5}$$

where E_{2D} is the 2D Young's modulus of monolayer graphene[10,11] and v is Poisson's ratio.

The total potential energy for the graphene bubble is then obtained as a function of the three kinematic parameters

$$\Pi(a, h, u_0) = 2\pi \int_0^a U(r) r \, dr - 2\pi(p - p_0) \int_0^a z(r) r \, dr,\tag{6}$$

where p is the pressure due to the gas molecules trapped inside the bubble and p_0 is the pressure outside the bubble.

For the bubble to be in equilibrium with a fixed radius a, we have

$$\frac{\partial \Pi}{\partial u_0} = \frac{\partial \Pi}{\partial h} = 0,\tag{7}$$

which leads to

$$h = \left[\frac{\phi(v)(p - p_0)a^4}{E_{2D}} \right]^{\frac{1}{3}}\tag{8}$$

and

$$u_0 = \left[\frac{\psi(v)(p - p_0)^2 a^5}{E_{2D}^2} \right]^{\frac{1}{3}},\tag{9}$$

with $\phi(v) = \frac{75(1-v^2)}{8(23+18v-3v^2)}$ and $\psi(v) = \frac{45(3-v)^3(1-v^2)^2}{8(23+18v-3v^2)^2}$.

By Eq. (8), the pressure inside the bubble can be determined from measurement of the bubble radius and central deflection, namely

$$p = \frac{E_{2D} h^3}{\phi a^4} + p_0.\tag{10}$$

Moreover, by the deflection profile in Eq. (1), the volume of the trapped gas in the bubble is

$$V = \frac{\pi}{2} a^2 h.\tag{11}$$

Thus, by the ideal gas law, the number of gas molecules inside the bubble may be estimated as

$$N = \frac{pV}{kT} = \frac{\pi}{2kT} \left(\frac{E_{2D} h^4}{\phi a^2} + p_0 a^2 h \right),\tag{12}$$

where k is Boltzmann constant and T is temperature.

With the number of gas molecules fixed inside the bubble, the potential energy can be obtained as a function of the bubble radius. Assuming $p \gg p_0$ (see results in Sec. IV A for justification), we obtain approximately

$$\Pi(a, N) = \frac{NkT}{4} - NkT\ln\frac{p_0 a^{5/2}}{(NkT)^{3/4}E_{2D}^{1/4}}. \quad (13)$$

The first term on the right hand side of Eq. (13) is the strain energy in graphene, which is independent of the bubble size under the condition of constant N. The second term is the potential energy of the gas, relative to the reference state in the ambient condition. As the bubble radius a increases, the total potential energy decreases. Meanwhile, the interfacial energy increases as part of the graphene is detached from the substrate. The equilibrium bubble radius is attained when the potential energy of the bubble is balanced by the adhesion energy (Γ) of the graphene/substrate interface, namely

$$\left(\frac{\partial \Pi}{\partial a}\right)_N = -2\pi a \Gamma, \quad (14)$$

which gives rise to the adhesion energy

$$\Gamma = \frac{5NkT}{4\pi a^2} = \frac{5E_{2D}h^4}{8\phi a^4}. \quad (15)$$

Hence, the adhesion energy can be determined from the measurements of the equilibrium bubble size (a and h). Note that, for the same adhesion energy, the equilibrium bubble size may vary, depending on N.

We note that the present membrane analysis is slightly different from Hencky's classical analysis,[12] which included 7 terms in a polynomial expansion of the deflection profile (as opposed to the two terms in Eq. (1)) with the coefficients determined numerically for specific Poisson's ratios. Table I compares Hencky's solution with the present membrane analysis for $v = 0.16$. Apparently, with same values of a, h, and E_{2D}, the present analysis underestimates the pressure and adhesion energy by 9% and 13%, respectively. A numerical error in Hencky's paper has been noted and corrected by others.[13–15] A subtle issue has also been raised regarding the difference between uniform lateral loading (Hencky's problem) and uniform pressure loading.[15] A more detailed analysis may be needed to settle these issues.

TABLE I. Comparison between the present analysis of graphene bubbles and Hencky's solution for $\nu = 0.16$.

	Normalized pressure $(p - p_0)/(\frac{E_{2D}h^3}{a^4})$	Adhesion energy $\Gamma/(\frac{E_{2D}h^4}{a^4})$
Hencky's solution	3.09	2.024
Present membrane analysis	2.825	1.766
Present nonlinear plate analysis ($h > 10$ nm)	2.518	1.049

III. A NONLINEAR PLATE MODEL

The bending stiffness of monolayer graphene is small but finite.[16–18] Moreover, the bending stiffness of monolayer graphene is an intrinsic property, independent of the in-plane elastic modulus. Nevertheless, a graphene monolayer may be treated as an elastic plate with specific moduli for in-plane and bending deformation. The von Karman nonlinear plate theory may be used in the analysis of graphene bubbles to take into account the effect of bending stiffness. Similar analyses have been carried out for thin film blisters, often by numerical methods.[8,19] Here, we present an approximate analytical solution similar to that of Timoshenko.[20] Treating the graphene monolayer as an elastic plate, the deflection profile is assumed to be

$$z(r) = h\left(1 - \frac{r^2}{a^2}\right)^2, \quad (16)$$

which satisfies the zero-slope boundary condition at the edge of the bubble (Fig. 1). In addition, the radial displacement is assumed to take the form

$$u(r) = r(a - r)(c_1 + c_2 r), \quad (17)$$

where c_1 and c_2 are two parameters to be determined. We note that the assumed deformation in Eqs. (16) and (17) is a reasonable approximation for small to moderately large bubbles.

By Eqs. (16) and (17), the radial and circumferential strain components are obtained as

$$\varepsilon_r = c_1(a - 2r) + c_2 r(2a - 3r) + \frac{8h^2 r^2(a^2 - r^2)^2}{a^8}, \quad (18)$$

$$\varepsilon_\theta = (a - r)(c_1 + c_2 r). \quad (19)$$

Again, the circumferential strain is zero at the edge ($r = a$).

The elastic strain energy consists of two parts, one due to stretching and the other due to bending. The elastic stretching energy per unit area of the membrane is

$$U_s(r) = \frac{E_{2D}}{2(1 - v^2)}(\varepsilon_r^2 + 2v\varepsilon_r\varepsilon_\theta + \varepsilon_\theta^2). \quad (20)$$

The elastic bending energy per unit area is

$$U_b(r) = \frac{D}{2}\left[\left(\frac{d^2 z}{dr^2}\right)^2 + \frac{1}{r^2}\left(\frac{dz}{dr}\right)^2 + \frac{2v}{r}\frac{dz}{dr}\frac{d^2 z}{dr^2}\right], \quad (21)$$

where D is the bending stiffness.

The total potential energy for the graphene bubble is then

$$\Pi(a, h, c_1, c_2) = 2\pi \int_0^a [U_s(r) + U_b(r)]r\,dr$$
$$- 2\pi(p - p_0)\int_0^a z(r)r\,dr. \quad (22)$$

At equilibrium, the two parameters c_1 and c_2 can be determined by setting $\frac{\partial \Pi}{\partial c_1} = \frac{\partial \Pi}{\partial c_2} = 0$, which yields

$$c_1 = \frac{(179 - 89v)}{126} \frac{h^2}{a^3}, \tag{23}$$

$$c_2 = \frac{(13v - 79)}{42} \frac{h^2}{a^4}. \tag{24}$$

Next, by setting $\frac{\partial \Pi}{\partial h} = 0$, we obtain that

$$p = 64\eta \frac{E_{2D} h^3}{a^4} + 64 \frac{Dh}{a^4} + p_0, \tag{25}$$

where $\eta = \frac{7505 + 4250v - 2791v^2}{211680(1-v^2)}$. Note that the first term on the right hand side of Eq. (25) is similar to the result from the membrane analysis in Eq. (10), while the second term is the contribution of the finite bending stiffness.

From the deflection profile in Eq. (16), the volume inside the bubble is

$$V = \frac{\pi}{3} a^2 h, \tag{26}$$

and thus the number of gas molecules is

$$N = \frac{pV}{kT} = \frac{\pi}{3kT} \left(64\eta E_{2D} \frac{h^4}{a^2} + 64D \frac{h^2}{a^2} + p_0 a^2 h \right). \tag{27}$$

Using the same equilibrium condition as in Eq. (14), we obtain the adhesion energy to be

$$\Gamma = \frac{80\eta E_{2D} h^4}{3a^4} + \frac{32Dh^2}{a^4}. \tag{28}$$

Again, the first term on the right hand side of Eq. (28) is similar to that obtained from the membrane analysis in Eq. (15), whereas the second term is due to the bending stiffness.

For a graphene bubble with a relatively small height ($h \ll a$), it may be sufficient to apply the linear plate analysis, which ignores the nonlinear terms in the strain energy as well as the contribution of stretch. As a result, the pressure inside the bubble is simply

$$p = \frac{64Dh}{a^4} + p_0. \tag{29}$$

Correspondingly, the adhesion energy of the graphene/substrate is obtained as

$$\Gamma = \frac{32Dh^2}{a^4}. \tag{30}$$

This is the exact solution to the linear plate equations.[8,20]

IV. DISCUSSIONS

A. Comparison of membrane and plate analyses

Figure 2 plots the pressure inside the bubble as a function of the central deflection. For comparison, we normalize the pressure according to the membrane analysis, i.e.,
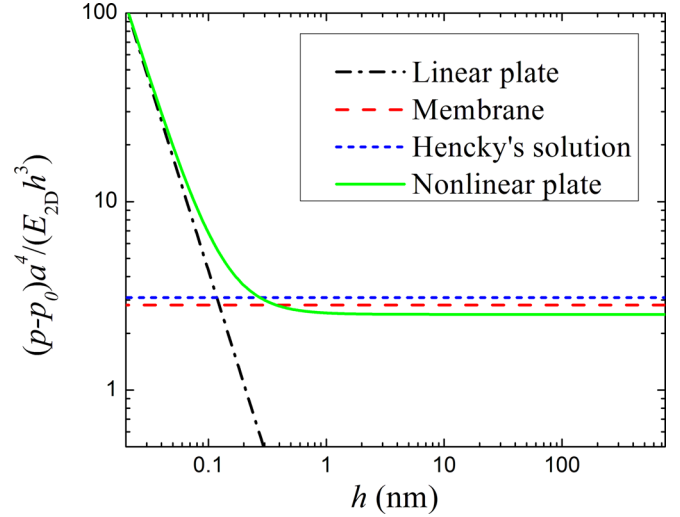

FIG. 2. Normalized pressure as a function of the central deflection, comparing four different solutions.

$\bar{p} = \frac{(p - p_0)a^4}{E_{2D} h^3}$, so that the normalized pressure is a constant by the membrane model. In contrast, in the linear plate solution (Eq. (29)), the normalized pressure decreases with increasing h. The nonlinear plate analysis on the other hand compares closely with the membrane analysis for large h and agrees with the linear plate solution for small h. The transition occurs at a length scale defined by the ratio between the bending modulus and the in-plane modulus: $L \sim \sqrt{\frac{D}{E_{2D}}}$, which is in the order of 0.1–1 nm. Such a small length scale suggests that the membrane analysis is generally sufficient for graphene bubbles with $h > 10$ nm. Here, we have used $E_{2D} = 353$ N/m, $v = 0.16$, and $D = 0.238$ nN-nm for monolayer graphene based on experimental measurements[10] and first-principle calculations.[16]

Recently, Georgiou *et al.*[2] measured the cross-sectional profile of a graphene bubble on an oxidized silicon substrate by atomic force microscope (AFM) in tapping mode. Figure 3 compares the experimental data with the deflection profiles assumed in the membrane and plate analyses. Apparently, the
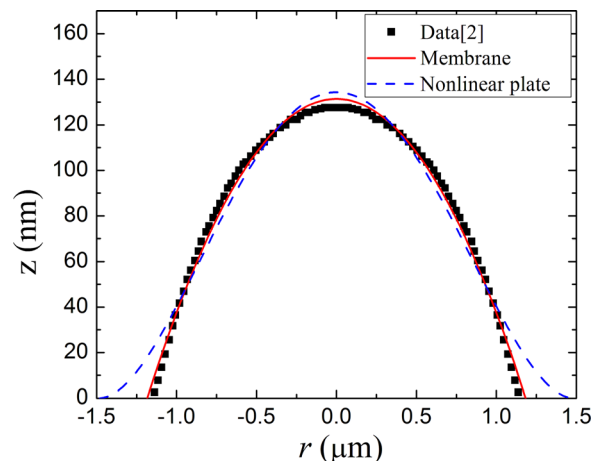

FIG. 3. Cross-sectional profile of a graphene bubble obtained from AFM measurements,[2] in comparison with the profiles obtained from the membrane and nonlinear plate analyses.

spherical profile in Eq. (1) offers a better fit to the data. Based on this, the bubble radius and central deflection are determined as $a = 1183$ nm and $h = 132$ nm. Using these values in Eq. (15), we obtain the adhesion energy $\Gamma = 0.097$ J/m^2. The pressure obtained from Eq. (10) is: $p = 1.272 \times 10^6$ Pa, and the number of gas molecules in the bubble is: $N = 8.92 \times 10^7$ (assuming $p_0 = 1.013 \times 10^5$ Pa and $T = 300$ K). The pressure inside the bubble is over 10 times of the ambient pressure (p_0), justifying the assumption made to reach Eq. (13).

B. Adhesion energy

Based on the membrane analysis, measuring the radius and central deflection of a graphene bubble is sufficient to determine the adhesion energy of the graphene/substrate interface. In addition, the number of gas molecules trapped inside the bubble can also be determined approximately by the ideal gas law. As shown in Fig. 4, for a fixed adhesion energy Γ, the central deflection of the bubble varies linearly with the bubble radius, according to Eq. (15). On the other hand, for a constant number of gas molecules (N), the central deflection varies with the radius nonlinearly according to Eq. (12). For a specific combination of Γ and N, the intersection of the two curves defines the equilibrium bubble radius and height. For comparison, the experimental data from Georgiou *et al.*[2] and Koenig *et al.*[6] are plotted in Fig. 4. The two data points from Georgiou *et al.*[2] give two relatively low adhesion energy values: $\Gamma = 0.097$ and 0.173 J/m^2. The data set from Koenig *et al.*[6] puts the adhesion energy in the range between 0.25 and 0.43 J/m^2, with an average value of 0.33 J/m^2. These values are lower than the reported value (0.45 J/m^2) for monolayer graphene on silicon oxide.[6] The difference is partly attributed to the approximations made in the present membrane analysis as opposed to Hencky's solution used by Koenig *et al.*[6] Note that the experiments by Koenig *et al.*[6] were performed with mechanically exfoliated graphene on predefined wells etched in SiO$_2$, where the radius of the bubble remains a constant ($\sim 2.5\,\mu$m) until a critical pressure was introduced inside the well. Beyond the critical pressure, the bubble radius increased stably and reached an equilibrium size under the condition of constant N; the measured bubble radius ($> 2.5\,\mu$m) and central

deflection were used to calculate the adhesion energy. The scattering of the adhesion energy from these data may suggest that the adhesion energy could be non-uniform due to the statistical nature of the surface roughness.[21] It was predicted that the effective adhesion energy between a graphene membrane and its substrate depends on surface roughness.[22] However, no quantitative measurement has been reported to correlate the adhesion energy of graphene with the surface roughness of its substrate.

Interestingly, Georgiou *et al.*[2] observed changes in the bubble size when a gate voltage (V_g) was applied. Figure 5(a) reproduces their data for gate voltages of 0, −15, −25, and −35 V, which were fitted here via Eq. (1) to determine the radius and central deflection of each bubble. The adhesion energy was then calculated and plotted in Fig. 5(b) as a function of the gate voltage. There was an apparent increase in adhesion energy as the magnitude of gate voltage increased. Since the intrinsic adhesion is not expected to depend on the gate voltage, this increase suggests that the attractive electrostatic interaction between the graphene and the substrate should be accounted for in the membrane analysis of the graphene bubble. A quantitative model of the electrostatic interaction may be brought up to further understand its contribution to the adhesion.[23,24] Also shown in Fig. 5(b) are the numbers of gas molecules estimated by Eq. (12). As
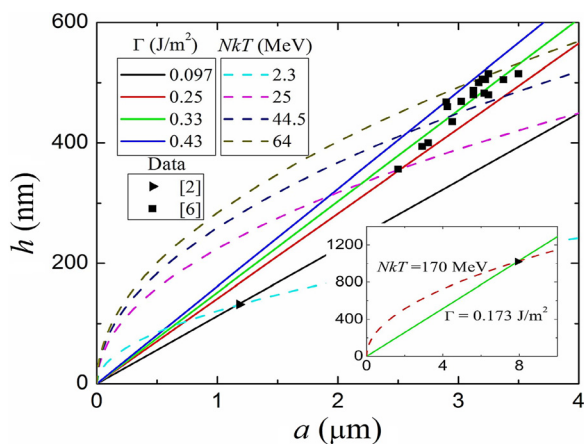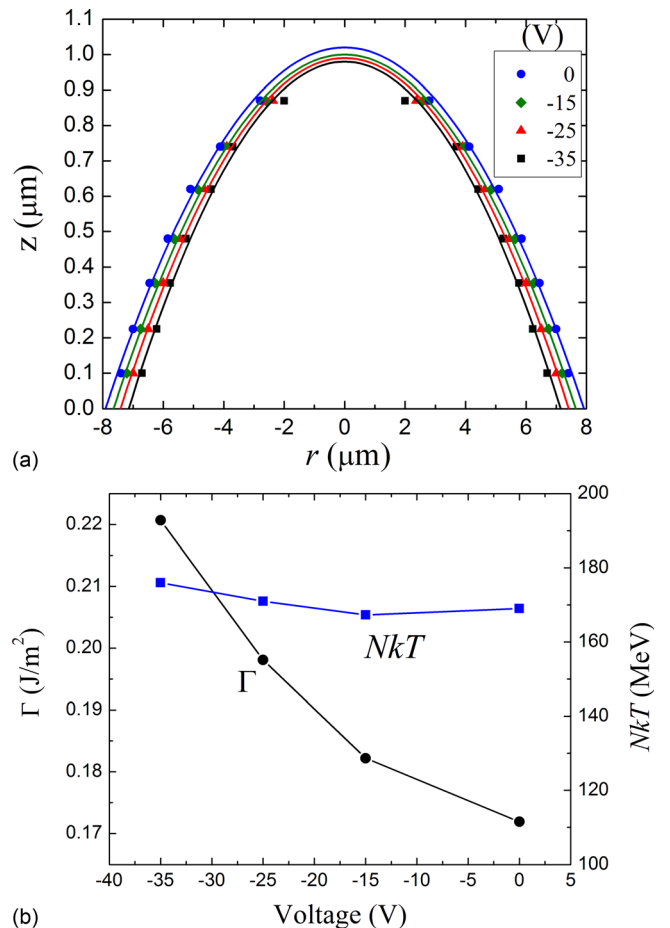
(a)

FIG. 4. Graphene bubble dimensions, central deflection vs. radius. Lines of constant adhesion energy and curves of constant NkT are drawn in comparison with experimental data.[2,6] The inset shows the data for a large bubble.[2]

(b)

FIG. 5. Effect of gate voltage: (a) cross-sectional profiles of a graphene bubble subject to gate voltage obtained from AFM[2] and fitting with Eq. (1); (b) The apparent adhesion energy and NkT versus the gate voltage.

expected, the number of gas molecules remains nearly a constant, independent of the gate voltage.

C. Strain distribution

Based on their AFM measurement (Fig. 3), Georgiou *et al.*[2] estimated the strain of the graphene bubble to be around 1%, which may be considered as the average radial strain along one diameter. Similar strain values were obtained from Raman spectroscopy measurements.[4] As indicated by the results of the membrane analysis and others,[12–15] the strain of a graphene bubble is generally non-uniform, with both radial and circumferential components, as given in Eqs. (3) and (4). The strain components, normalized by $\sqrt{\Gamma/E_{2D}}$, are plotted in Figure 6 as a function of r/a. At the center ($r = 0$), the strain is equi-biaxial ($\varepsilon_r = \varepsilon_\theta$). At the edge of the bubble ($r = a$), the strain is uniaxial as $\varepsilon_\theta = 0$. While the circumferential strain varies linearly from the center to the edge, the radial strain is nonlinear in between. Remarkably, the magnitude of the strain as predicted by the membrane analysis scales linearly with $\sqrt{\Gamma/E_{2D}}$, independent of the bubble size. This suggests that strain measurement could be used as an alternate approach for determining the adhesion energy. Figure 7 plots the strain as a function of the adhesion energy. To compare with the AFM measurement, we calculate the average radial strain along one diameter and obtain (for $v = 0.16$)

$$\varepsilon_r^{la} = 0.508 \sqrt{\Gamma/E_{2D}}. \tag{31}$$

With $\varepsilon_r^{la} = 1\%$,[2,4] we obtain $\Gamma = 0.14\,\text{J/m}^2$, in close agreement with the adhesion energy obtained earlier based on the measured bubble dimensions.

Raman spectroscopy may be used to measure the local strain based on the fact that strain modifies the crystal phonon frequency due to the anharmonic interactions among the atoms. The method has been used extensively for measuring strain and stress in silicon.[25–28] The Raman spectrum of monolayer graphene typically has four peaks, the so-called D, G, 2D, and 2D′ peaks, in the order of increasing frequency.[4] Subject to a state of strain with two principal components ε_1 and ε_2, the frequency shift of each peak is
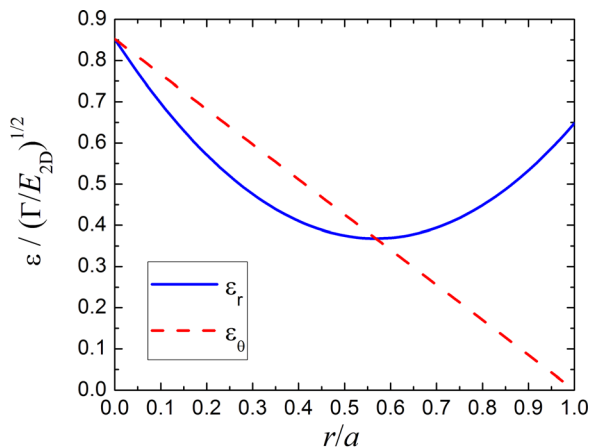

FIG. 6. Variation of the radial and circumferential strain components in a graphene bubble.
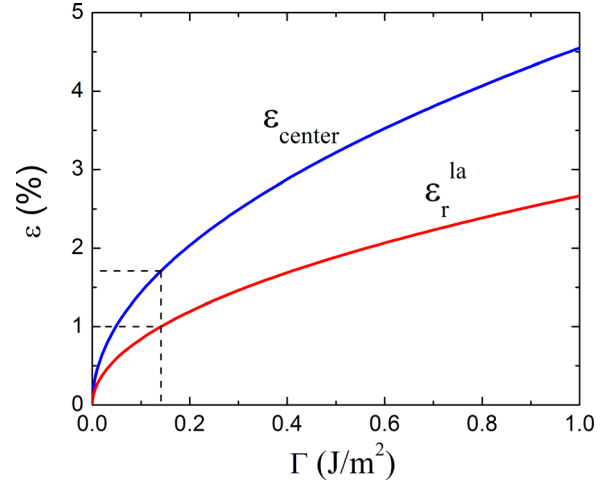

FIG. 7. Dependence of the local strain at the center and the linear average radial strain on the adhesion energy for monolayer graphene bubbles.

$$\Delta\omega = -\gamma\omega_0(\varepsilon_1 + \varepsilon_2)\pm\frac{1}{2}\beta\omega_0(\varepsilon_1 - \varepsilon_2), \tag{32}$$

where ω_0 is the reference frequency at zero strain, γ is the so-called Gruneisen parameter, and β is the shear deformation potential.[29] The second term on the right hand side of Eq. (32) gives the mode splitting due to the shear component of the strain, as observed for the G peak of graphene under uniaxial strain.[29–31] Both the Gruneisen parameter and the shear deformation potential have been predicted from first-principle calculations,[29] with which the local strain of graphene can be measured by Raman spectroscopy.

In an effort to experimentally determine the Gruneisen parameters of graphene, Zabel *et al.*[4] carried out Raman spectroscopy measurements of graphene bubbles. Since the strain is equibiaxial ($\varepsilon_r = \varepsilon_\theta$) at the center of the bubble, no splitting of the G peak was observed, while the Raman spectrum was strongly blue-shifted compared to the reference spectrum measured for unstrained graphene. To determine the Gruneisen parameters, an independent measurement of the strain is needed. Zabel *et al.*[4] used the average radial strain measured by AFM, which was approximately 1%. As shown in Fig. 6, the strain is non-uniform. The local strain at the center of the bubble is considerably higher than the average strain (Fig. 7). For $v = 0.16$, the local strain at the center of the bubble is

$$\varepsilon_{center} = 0.855 \sqrt{\Gamma/E_{2D}}, \tag{33}$$

which is about 17% higher than the average radial strain ε_r^{la} in Eq. (31). Thus, for a bubble with $\varepsilon_r^{la} = 1\%$, the local strain $\varepsilon_{center} = 1.68\%$. Using this local strain value, along with the Raman shifts measured by Zabel *et al.*[4] ($\Delta\omega = -57, -140, -108,$ and $-68\,\text{cm}^{-1}$ for the G, 2D, 2D′, and D peaks; $\omega_0 = 1582, 2692, 3245,$ and $1349\,\text{cm}^{-1}$), we obtain the Gruneisen parameters: $\gamma(G) = 1.07$, $\gamma(2D) = 1.55$, $\gamma(2D') = 0.99$, and $\gamma(D) = 1.50$. These values are considerably lower than the values obtained by Zabel *et al.*[4] as well as those predicted by the first-principle calculations.[29] The cause of this discrepancy is not known. While the theoretical model of the graphene

bubble could be improved to more accurately predict the strain, it is desirable to independently measure the local strain components along with the Raman spectroscopy in order to determine the Gruneisen parameters fully by experiments. Moreover, the effects of the laser power and the laser spot size may also be investigated. For example, laser heating may alter the strain of graphene locally, and the non-uniform strain distribution within the laser spot size may require the use of an average strain over the area under the laser spot.

Strain engineering has been suggested as a viable approach to tailoring the electronic properties of graphene.[3,32,33] For this purpose, a relatively large strain (>5%) is needed.[34] Figure 7 shows that the strain of a graphene bubble is limited by the adhesion energy. To achieve a 5% strain at the center of the bubble, the required adhesion energy is predicted to be 1.2 J/m², much higher than the measured adhesion energy of graphene on SiO₂ and other substrate materials.[6,7,35] Surface functionalization may be used to enhance the adhesion so that graphene bubbles with higher strain can be achieved.

D. Transport of gas molecules

Stolyarova *et al.*[1] observed coalescence of graphene bubbles during annealing, which can be understood as a result of the transport of gas molecules along the interface driven by the different pressures in bubbles of different sizes. Combining Eqs. (10) and (15), the membrane model predicts that the pressure inside the graphene bubble is inversely proportional to the bubble radius

$$p = \frac{1}{a}\left(\frac{8^3 E_{2D}\Gamma^3}{125\phi}\right)^{1/4}. \tag{34}$$

Consequently, the pressure is higher in the smaller bubbles and the pressure difference drives the gas molecules to diffuse from smaller bubbles to larger bubbles. The diffusion process is kinetically mediated and is enhanced by thermal annealing so that the large bubbles grow larger while the small bubbles disappear, similar to the Ostwald ripening process in thin film growth.[36]

The coalescence of graphene bubbles may also be understood from an energy consideration. With Eqs. (13) and (15), the free energy of each bubble can be determined as a function of the number of gas molecules:

$$F(N) = \Pi(N) + \pi a^2 \Gamma$$

$$= \frac{3}{2}NkT\left(1 - \frac{1}{3}\ln\left[NkT\left(\frac{0.0387\phi p_0^4}{E_{2D}\Gamma^5}\right)^{1/2}\right]\right). \tag{35}$$

It can be shown that the free energy of two small bubbles is greater than the free energy of one large bubble with the same total number of gas molecules, namely

$$F(N_1) + F(N_2) > F(N_1 + N_2). \tag{36}$$

Therefore, there exists a thermodynamic driving force for the two small bubbles to coalesce so that the total free energy

is reduced. In other words, while each graphene bubble is in a thermodynamically equilibrium state, the system with a group of graphene bubbles is not in equilibrium. Since the graphene is impermeable,[5] the kinetic pathways for the transport of gas molecules may include the graphene/substrate interface and the substrate bulk. For example, Koenig *et al.*[6] utilized the bulk diffusion of nitrogen molecules through SiO₂ to pressurize graphene membranes. However, bulk diffusion is typically slow and the most likely route for the coalescence of graphene bubbles in the time frame of the experiments is interfacial diffusion.

E. Effect of van der Waals interaction

It is commonly assumed that the interfacial adhesion between graphene and an amorphous oxide substrate is through van der Waals interaction.[37–40] By assuming an equilibrium separation between the graphene and the substrate along with an adhesion energy, a simple model of the van der Waals interaction predicts the traction-separation relation for the graphene/substrate interface.[38] Such a model could be employed to study the adhesive interaction near the edge of a graphene bubble, which has been ignored in the present study. Since the equilibrium separation is in the order of 0.4 nm,[21] the adhesive interaction decays quickly as the separation exceeds a few nanometers. Therefore, for relatively large graphene bubbles (h > 10 nm), the effect is negligible. However, for nanoscale graphene bubbles,[1,3] the adhesive interaction could be significant not only near the edge but also over the entire bubble. Consequently, the shape of graphene nanobubbles may be different and depend on the traction-separation relation of the interface, which is left for future studies.

V. SUMMARY

The mechanics of graphene bubbles is analyzed by using membrane and nonlinear plate theories. A comparison of the two theoretical analyses suggests that the membrane analysis is sufficient for relatively large bubbles (h > 10 nm). A simple solution relates the bubble size (radius and central deflection) to the adhesion energy between graphene and its substrate. This membrane analysis was applied to reported experimental data, and adhesion energies ranging from 0.097 to 0.43 J/m² were extracted for mechanically exfoliated graphene on silicon oxide. The wide range of values may be partly attributed to the effect of surface roughness. A non-uniform, biaxial strain distribution is predicted for the graphene bubble, in comparison with experimental measurements by AFM (average radial strain) and Raman spectroscopy (local strain). The mechanics of graphene bubbles is then extended to discuss transport of gas molecules among graphene bubbles of different sizes and coalescence of graphene bubbles from a thermodynamics perspective.

The present study is confined to relatively large graphene bubbles (h > 10 nm), for which adhesive interactions are accounted for via an energy balance involving the strain and adhesion energies, without a detailed analysis incorporating the adhesive interaction via a traction-separation relation. In addition, only the monolayer graphene bubbles are considered, although the approach can be readily extended to

the study of multilayer graphene bubbles. Further studies may also consider the effect of residual stress and possibly anisotropic shapes of graphene bubbles.[2,3]

ACKNOWLEDGMENTS

[1]E. Stolyarova *et al.*, Nano Lett. **9**, 332–337 (2009).
[2]T. Georgiou *et al.*, Appl. Phys. Lett. **99**, 093103 (2011).
[3]N. Levy *et al.*, Science **329**, 544–547 (2010).
[4]J. Zabel *et al.*, Nano Lett. **12**, 617–621 (2012).
[5]J. S. Bunch *et al.*, Nano Lett. **8**, 2458–2462 (2008).
[6]S. P. Koenig, N. G. Boddeti, M. L. Dunn, and J. S. Bunch, Nat. Nanotechnol. **6**, 543–546 (2011).
[7]Z. Zong, C.-L. Chen, M. R. Dokmeci, and K.-T. Wan, J. Appl. Phys. **107**, 026104 (2010).
[8]L. B. Freund and S. Suresh, *Thin Film Materials* (Cambridge University Press, 2003).
[9]Y. Huang, J. Wu, and K. C. Hwang, Phys. Rev. B **74**, 245413 (2006).
[10]C. Lee, X. Wei, J. W. Kysar, and J. Hone, Science **321**, 385–388 (2008).
[11]Q. Lu and R. Huang, Int. J. Appl. Mech. **1**, 443–467 (2009).
[12]H. Hencky, Z. Math. Phys. **63**, 311–317 (1915).
[13]J. D. Campbell, Q. J. Mech. Appl. Math. **9**, 84–93 (1956).
[14]J. G. Williams, Int. J. Fract. **87**, 265–288 (1997).
[15]W. B. Fichter, NASA Technical Paper 3658, 1997.
[16]K. N. Kudin, G. E. Scuseria, and B. I. Yakobson, Phys. Rev. B **64**, 235406 (2001).
[17]Q. Lu, M. Arroyo, and R. Huang, J. Phys. D: Appl. Phys. **42**, 102002 (2009).
[18]P. Koskinen and O. O. Kit, Phys. Rev. B **82**, 235420 (2010).
[19]K. M. Liechti and A. Shirani, Int. J. Fract. **67**, 21–36 (1994).
[20]S. Timoshenko, *Theory of Plates and Shells* (McGraw-Hill, New York, 1940), pp. 333–337.
[21]M. Ishigami *et al.*, Nano Lett. **7**, 1643–1648 (2007).
[22]W. Gao and R. Huang, J. Phys. D: Appl. Phys. **44**, 452001 (2011).
[23]J. Sabio *et al.*, Phys. Rev. B **77**, 195409 (2008).
[24]G. Duan and K.-T. Wan, J. Appl. Mech. **74**, 927–934 (2007).
[25]Q. Ma, S. Chiras, D. R. Clarke, and Z. Suo, J. Appl. Phys. **78**, 1614–1622 (1995).
[26]I. DeWolf, H. E. Maes, and S. K. Jones, J. Appl. Phys. **79**, 7148–7156 (1996).
[27]P. A. Gustafson, S. J. Harris, A. E. O'Neill, and A. M. Waas, J. Appl. Mech. **73**, 745–751 (2006).
[28]S.-K. Ryu, Q. Zhao, M. Hecker, H. Y. Son, K. Y. Byun, J. Im, P. S. Ho, and R. Huang, J. Appl. Phys. **111**, 063513 (2012).
[29]T. M. G. Mohiuddin *et al.*, Phys. Rev. B **79**, 205433 (2009).
[30]M. Huang *et al.*, Proc. Natl. Acad. Sci. U.S.A. **106**, 7304 (2009).
[31]M. Mohr *et al.*, Phys. Rev. B **82**, 201409 (2010).
[32]V. M. Pereira and A. H. Castro Neto, Phys. Rev. Lett. **103**, 046801 (2009).
[33]F. Guinea, M. I. Katsnelson, and A. K. Geim, Nat. Phys. **6**, 30–33 (2010).
[34]J. S. Bunch and M. L. Dunn, Solid State Commun. **152**, 1359–1364 (2012).
[35]T. Yoon, W. C. Shin, T. Y. Kim, J. H. Mun, T.-S. Kim, and B. J. Cho, Nano Lett. **12**, 1448–1452 (2012).
[36]M. Ohring, *Materials Science of Thin Films* (Academic, 2002).
[37]Z. Lu and M. L. Dunn, J. Appl. Phys. **107**, 044301 (2010).
[38]Z. H. Aitken and R. Huang, J. Appl. Phys. **107**, 123531 (2010).
[39]Z. Xu and M. J. Buehler, J. Phys.: Condens. Matter **22**, 485301 (2010).
[40]Z. Zhang and T. Li, J. Appl. Phys. **110**, 083526 (2011).